NJC

Accepted Manuscript

This is an *Accepted Manuscript*, which has been through the Royal Society of Chemistry peer review process and has been accepted for publication.

Accepted Manuscripts are published online shortly after acceptance, before technical editing, formatting and proof reading. Using this free service, authors can make their results available to the community, in citable form, before we publish the edited article. We will replace this *Accepted Manuscript* with the edited and formatted *Advance Article* as soon as it is available.

You can find more information about *Accepted Manuscripts* in the Information for Authors.

Please note that technical editing may introduce minor changes to the text and/or graphics, which may alter content. The journal's standard Terms & Conditions and the Ethical guidelines still apply. In no event shall the Royal Society of Chemistry be held responsible for any errors or omissions in this *Accepted Manuscript* or any consequences arising from the use of any information it contains.

ROYAL SOCIETY OF CHEMISTRY

www.rsc.org/njc

Synthesis, DNA interaction and anticancer activity of 2-anthryl substituted benzimidazole derivatives

Vyankat A. Sontakke[a], Anup N. Kate[b], Sougata Ghosh[c], Piyush More[c], Rajesh Gonnade[d], Navanath M. Kumbhar[e], Anupa A. Kumbhar[b], Balu A. Chopade[c] and Vaishali S. Shinde[a*]

[a]*Garware Research Centre, Department of Chemistry, Savitribai Phule Pune University (formerly University of Pune) Pune-411007, India*

[b]*Department of Chemistry, Savitribai Phule Pune University (formerly University of Pune) Pune-411007, India*

[c]*Institute of Bioinformatics and Biotechnology, Savitribai Phule Pune University (formerly University of Pune) Pune-411007, India*

[d]*Centre for Materials Characterization, National Chemical Laboratory, Dr. Homi Bhabha Road, Pashan, Pune-411008, India*

[e]*Rajiv Gandhi Institute of Information Technology and Biotechnology, Bharati Vidyapeeth Deemed University, Pune-411046, India*

**Corresponding author.* Fax: +91-20-25691728. *Email address:* vsshinde@chem.unipune.ac.in; vaishali.san@gmail.com (Vaishali S Shinde).

Abstract

The 2-anthryl benzimidazole derivatives (**5**-**7**) with hydrogen, carboxyl and benzoyl substituents at 5th-position have been synthesized using silica supported periodic acid catalyst. DNA cleavage activity of **5**-**7** studied in presence of light using pBR322 plasmid DNA showed that cleavage activity varies with substitution at 5th-position of benzimidazole derivatives. DNA binding studies using ethidium bromide displacement assay demonstrated non-intercalative binding mode of **5**-**7.** Anticancer activity of these target molecules were tested against MCF-7

and HL-60 cell lines and exhibited remarkable activity in micromolar range. Cellular uptake and morphological changes were confirmed by fluorescence and confocal microscopy. Molecular docking study was carried out to explore the DNA binding mechanism with **5**-**7**.

1. Introduction

Bioactive small molecules may interact with DNA *via* different binding modes. Therefore the interactions of these molecules with DNA are of great interest. Benzimidazole; a nitrogen containing aromatic heterocycle is a key component in various biologically important molecules[1] encompassing broad spectrum of activities like anticancer,[2] antiviral,[3] antimicrobial[4] and antifungal[5]. Different chemotherapeutic anticancer drugs interact directly with DNA or prevent the appropriate relaxation of DNA through inhibition of topoisomerases.[6] Hoechst 33258 [2′-(4-hydroxyphenyl)-5-(4-methylpiperazinyl)-2,5′-bi-1H-benzimidazole] and Hoechst 33342 [2′-(4-ethoxyphenyl)-5-(4-methylpiperazinyl)-2,5′-bi-1H-benzimidazole] are topoisomerase I (topo-I) inhibitors and showed binding to DNA in the minor groove with specificity to A-T region.[7] Studies have been reported to assess the effects of substitution at 5th-position of benzimidazoles (as shown in Fig. 1**a**) with respect to their ability to act as topo-I inhibitors.[8] Similarly, the influence of structural variation at 2nd-position on topo-I inhibition and cytotoxicity have also been reported.[9] Good DNA interaction ability exhibits better cytotoxicity[10] and DNA photocleavage activity. Such molecules have proved useful in photodynamic therapy (PDT).[11] Anthracene derivatives have been investigated for their DNA binding and photocleavage activity. Kumar and coworkers studied DNA binding and photocleavage activities of anthracene derivatives with substitution at 9th-positions (as shown in Fig. 1**b)** and proved the influence of substitution on the DNA interactions.[12] A series of polyamines bearing two or more anthryl rings were synthesized and studied for their DNA/RNA binding by Schneider and coworkers[13]

However, Grant and coworkers reported DNA binding and metal-activated photo-cleavage ability of several bi-functional compounds with rigid aromatic spacers.[14] Recently, monoanthryl and bisanthryl compounds were synthesized and studied for their DNA binding abilities[15]. Anthracene itself was shown to be active against psoriasis.[16] Pseudourea was the first anthracene derivative tested in clinical trials.[17] Ametantrone[18] mitoxantrone[19] and bisantrene[20] were the other anthracene derivatives tested for their anticancer activity. All of these exert their effect by binding to DNA through either groove/electrostatic or intercalative binding modes.

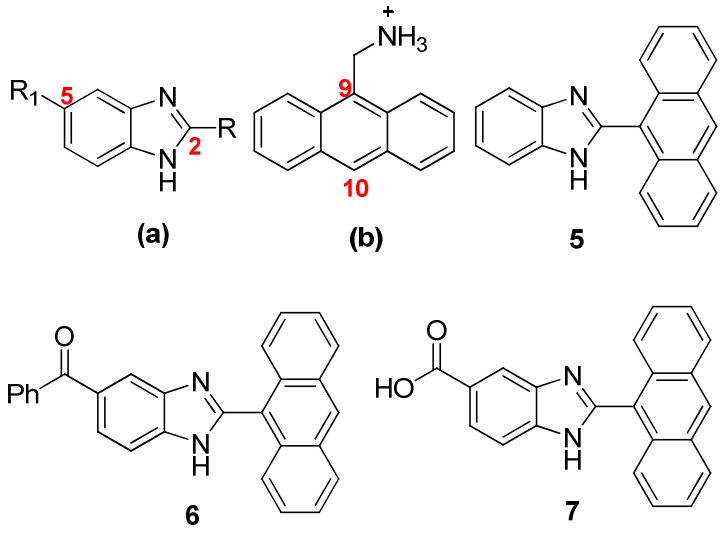

Fig. 1 Structures of substituted benzimidazole and anthracene derivative.

In view of wide applications of benzimidazole and anthracene moiety in drug development, we planned to synthesize the molecules having both the units together attached at appropriate positions expecting enhanced biological activities especially, DNA interactions. With this aim, we synthesized 2-anthryl benzimidazoles **5-7** (Fig. 1) and studied their interaction with DNA. Further these compounds were tested for anticancer activity against MCF-7, HL60 cell lines and studied for molecular docking.

2. Experimental

2.1. Materials and methods

All reactions were performed in open atmosphere without further purification of reagents and distilled solvents. Thin-layer chromatography (TLC) was performed using 0.25 mm silica gel coated plates. Column chromatography was performed using hexane: ethyl acetate solvent and silica gel (100-200 mesh). ^{1}H NMR (300 MHz) and ^{13}CNMR (75 MHz) spectra were recorded on Varian Mercury instrument with DMSO-d_6 as the solvent. Chemical shifts were reported in δ unit (ppm) with reference to TMS as an internal standard and J values were given in Hertz. Melting points were determined on Thomas Hoover capillary melting point apparatus and are uncorrected. IR spectra were recorded on a Shimadzu FTIR 8400 spectrophotometer in KBr and expressed in cm^{-1}. Elemental analyzes were carried out with Thermo-Electron Corporation CHNS analyzer Flash-EA 1112. High resolution mass spectra were recorded on Bruker Daltonics microTOF-Q using electrospray ionization.

2.2. Synthesis of silica supported H_5IO_6 catalyst (H_5IO_6-SiO_2).

In a 15ml hot water (60 °C), H_5IO_6 (2.50 g, 10.96 mmol) was dissolved in a 50 mL round-bottom flask. Silica gel (230-400 mesh, 10 g) was added with constant stirring. The obtained H_5IO_6 (resultant mixture contains 20 wt% of H_5IO_6) supported with silica gel was dried in oven at 100^{o}C for 12h to obtain a white free flow powder.

2.3. General procedure for synthesis of benzimidazoles

A typical procedure is as follows: A mixture of 1,2-phenylenediamine **1** (108mg, 1.0mmol), 9-anthraldehyde **4** (206mg, 1.0mmol) in acetonitrile (5.0mL) was taken, and H_5IO_6

(45mg, 20mmol% supported on silica 210mg) was added at room temperature. The reaction was stirred at room temperature. After completion of the reaction (monitored by TLC), the reaction mixture was filtered over celite. The filtrate was evaporated under vacuum and subsequently dried to afford crude product which was purified by column chromatography using hexane/ethylacetate as eluent to afford pure benzimidazole **5** (209mg, 71%).

2.3.1. 2-(Anthracen-10-yl)-1H-benzo[d]imidazole (5).[21]

White solid; mp 262-264 °C; IR (cm^{-1}, KBr): 3051, 2918, 1620, 1400, 1228, 925, 848, 740. ^{1}H NMR (300 MHz, DMSO-d_6): δ 13.02 (brs, 1H), 8.79 (s, 1H), 8.18 (d, J = 7.2Hz, 2H), 7.71 (d, J = 8.1Hz, 4H), 7.50 (m, 4H), 7.31 (s, 2H); ^{13}C NMR (75 MHz, DMSO-d_6): δ 149.5, 130.6, 130.5, 128.8, 128.4, 126.7, 125.7, 125.5, 122.0; (Found: C, 85.67; H, 4.75; N, 9.50. Cal for $C_{21}H_{14}N_2$: C, 85.69; H, 4.79; N, 9.52%).

2.3.2. 2-(Anthracen-10-yl)-1H-benzo[d]imidazol-5-yl)(phenyl)methanone (6).

Yellow solid, 64% yield; mp 107-109 °C;IR (cm^{-1}, KBr): 3055, 1784, 1647, 1527, 1404, 1298, 893, 732; ^{1}H NMR (300 MHz, DMSO-d_6): δ 13.49 (brs, 1H), 8.87 (s, 1H), 8.23 (d, J = 8.3Hz, 2H), 7.84-7.82 (m, 3H), 7.71-7.68 (m, 4H), 7.62-7.51 (m, 7H); ^{13}C NMR (75 MHz, DMSO-d_6): δ 195.9, 138.1, 132.2, 130.6, 130.4, 129.5, 129.3, 128.6, 128.5, 127.2, 125.8, 125.3, 124.9; (Found: C, 84.35; H, 4.53; N, 6.99. Cal for $C_{28}H_{18}N_2O$: C, 84.40; H, 4.55; N, 7.03%). HRMS (ESI) m/z calcd. for $C_{28}H_{19}N_2O$ $(M + H)^+$ 399.1497, found 399.1500.

2.3.3. 2-(Anthracen-10-yl)-1H-benzo[d]imidazole-5-carboxylic acid (7).

White solid, 62% yield; mp 248-250 °C; IR (cm^{-1}, KBr): 3051, 1697, 1622, 1398, 1338, 1224, 893, 734. ^{1}H NMR (300 MHz, DMSO-d_6): δ 13.31 (brs, 1H), 12.69 (brs, 1H),8.77 (s, 1H), 8.34 (brs, 1H), 8.13 (d, J = 8.2 Hz, 2H), 7.87 (m, 2H), 7.61 (d, J = 8.2 Hz, 2H), 7.51-7.41 (m, 4H); ^{13}C NMR (75 MHz, DMSO-d_6): δ 167.9, 151.5, 146.8, 143.3, 137.8, 134.2, 130.5, 130.3,

129.1, 128.5, 127.0, 126.2, 125.6, 125.3, 125.0, 124.4, 123.9, 122.9, 120.9, 118.7, 113.3, 111.3; (Found: C, 78.01; H, 4.18; N, 8.25. Cal. for $C_{22}H_{14}N_2O_2$: C, 78.09; H, 4.17; N, 8.28%; HRMS (ESI) m/z calcd. for $C_{22}H_{15}N_2O_2$ $(M + H)^+$ 339.1134, found 339.1127.

2.4. Single crystal development

5 was dissolved in hot (~ 55°C) methanol/ DMF (9:1 v/v) to obtain clear solution. On slow evaporation of solvent at room temperature (20-25°C), good quality crystals suitable for X-ray diffraction were obtained in about 20 days.

2.4.1. Crystal data

X-ray intensity data measurements of **5** was carried out on a Bruker SMART APEX II CCD diffractometer with graphite-monochromatized (MoK_α= 0.71073Å) radiation at room temperature 298(2) K. The X-ray generator was operated at 50 kV and 30 mA. A preliminary set of cell constants and an orientation matrix were calculated from 1052 reflections harvested from three sets of 36 frames (12 frames from each set). The optimized strategy used for data collection consisted of two $\varphi$and one ω scan sets, with 0.5° steps in φorω;completeness achieved was 100% with redundancy 4.00. Data were collected with a frame time of 20 sec keeping the sample-to-detector distance fixed at 5.00 cm. A total of 739 frames were collected. The X-ray data collection was monitored by APEX2 program (Bruker, 2006).[22] Final unit cell parameters were obtained from 3132 reflections after integration. All the data were corrected for Lorentzian, polarization and absorption effects using SAINT and SADABS programs (Apex2, Bruker, 2006). SHELX-97 was used for structure solutionand full matrix least-squares refinement on F^2.[23] All the hydrogen atoms were placed in geometrically idealized positionand constrained to ride on their parent atoms.

2.5. DNA binding by ethidium bromide displacement assay

We prepared the concentrated stock solutions of **5**-**7** in DMSO and diluted in such a way that DMSO concentration was 10% (v/v) .Fluorescence quenching experiments were carried out by the successive additions of 0 -50 μM of **5**-**7** to the DNA (10 μM) solutions containing 10 μM ethidium bromide (EtBr) in phosphate buffer. The changes in fluorescence intensities at 585 nm (545 nm excitation) of EtBr bound to DNA were recorded.

2.6. DNA cleavage studies

For the gel electrophoresis experiment, pBR322 plasmid DNA (100 ng) was incubated with **5**-**7** in Tris-boric acid-EDTA (TBE) buffer of pH 8.2 and the solutions were incubated in dark for 20 min at 37^{o}C before irradiation with monochromatic light of 365 nm for 1h. The samples were analyzed by 1% agarose gel electrophoresis for 2.5 h at 60V in TBE buffer and photographed using AlphaInnotech gel documentation system after staining with 0.5 μg/mL ethidium bromide. The extent of cleavage of the SC DNA was determined by measuring the intensities of the bands using the AlphaInnotech gel documentation system (AlphaImager 2200). For mechanistic investigations, experiments were carried out in the presence of different radical scavenging agents. These reactions were carried out by adding scavenging agents such as DMSO, mannitol, DABCO, L-histidine, and SOD to SC DNA prior to the addition of the complexes. Samples were incubated for 30 min at 37^{o}C. The concentrations of scavenging agents given correspond to stock concentration. One microliter of stock solution was added to make the total reaction volume 10 μL.

2.7. MTT assay

Anticancer activity of the benzimidazoles was tested against two cancer cell lines, MCF-7 (human breast adenocarcinoma) and HL-60 (human promyelocytic leukemia). MCF-7 was cultured in DMEM while HL-60 cells were cultured in RPMI1640 medium supplemented with 10% fetal bovine serum under humidified atmosphere (37 °C, 5% CO_2). **5-7** were evaluated *in vitro* at a concentration range of 1 μM to 50 μM. The MTT colorimetric assay was used to determine growth inhibition with cisplatin as a reference standard. 100 μl of cell suspension ($5x10^6$ cells/mL) were plated in 96-well plates and allowed to attach for 24 h. The compounds were dissolved in 10 % DMSO. Cells were exposed in triplicate wells to these derivatives at various concentrations for 48 h and watched under fluorescent microscope. After 48 h, 20 μL MTT (3-(4,5-dimethyl-thiazol-2-yl)-2,5-diphenyl-tetrazolium bromide) solution (5 mg/mL) was added to each well. After 4 h of incubation, 100 μL solubilization buffer (10% SDS in 0.01 M HCl) was added to dissolve the formazan precipitate. Plates were incubated overnight and absorbance at 570 nm was determined on a microplate reader (SpectraMax M5, Molecular Devices Corp, USA). The absorbance values were used to calculate % inhibition at various concentrations and IC_{50} values.

2.8. Fluorescence and confocal microscopy

MCF7 cells were seeded onto glass coverslips and incubated for 24 h for attachment followed by a treatment with **6** and **7** as they showed superior activity at a dose equivalent to the IC_{50} values. After incubation for 48 h the cells were washed with PBS to remove any excessive free compounds. Cells then fixed in 4% para-formaldehyde (PFA) followed by staining with propidium iodide (PI) and 4′,6-diamidino-2-phenylindole (DAPI). Samples were viewed initially

under fluorescent microscope followed by confocal microscope using Zeiss LSM510 META confocal microscope at 60X magnification (4x zoom).

2.9. Automated complete geometry optimizations and Molecular Electrostatic Potentials (MEPs) calculations

In order to understand the structural behavior of synthesized 2-anthryl substituted benzimidazoles, geometry optimizations have been performed using quantum chemical semi-empirical methods such as RM1, PM6, PM3, AM1 and MNDO methods.[24-27] Geometrical salient features have also been tested using HF-SCF using 6-31G** basis set and Density Functional Theory (DFT) by using B3LYP/6-31G** basis set.[28-29] Molecular electrostatic potentials of **5-7** were predicted using DFT method.[29] All energy calculations performed on *Spartan '14* (Wavefunction, Inc) software.[30] Initial geometry for **5-7** adopted from crystallographic data of **5**, while substituent were added to build **6** and **7** using *Spartan'14*[30]. Fig. 13S depicted the nomenclature and conventional numbering system for **5-7** describing torsion angles such as α, β and γ. Torsion angle α [C(9)-C(8)-C(7)-N(1)] is describing rotation around the bond C(8)–C(7) and measures the orientation of bond C(7) and N(1) with respect to C(9)-C(8) from the cis (eclipsed,0°) position in the right hand sense of rotation. Likewise the torsion angles β [C(2)-C(3)-C(22)-O(2)] and γ [C(3)-C(22)-O(2)-H] defines the rotation of the successive chemical bonds. Torsion angle α for **5-7** maintained from crystallographic data, whereas for **6** and **7** β and γ torsion angles are adopted as 180°.

2.9.1. Molecular docking Procedure

Molecular docking studies of **5-7** with DNA molecule have been performed using Autodock software.[31] Crystal structure of DNA dodecamer (1BNA.pdb) having sequence

d(CpGpCpGpApApTpTpCpGpCpG) was downloaded from protein data bank (www.rcsb.org) and used for docking studies. Docking procedure was employed from earlier studies.[32-34] **5-7** were geometrically optimized using DFT method prior to docking studies. Similarly, DNA structure was refined by removing non-polar hydrogen atoms and adding Kollman united atom charges and polar hydrogen atoms. Gasteiger charges and hydrogen atoms were added to **5-7** using Autodock wizard.[31] AutoGrid module was used for calculating the grid maps and centered on the ligand binding site of DNA, in such a way that it would totally cover the ligand molecules (**5-7**). The grid size was set to 54 A° × 54 A° × 76 A° with a grid spacing 0.375 A°. The step size of 1Å for translation and the maximum number of energy evaluation was set to 2,500,000. The 100 runs were performed. For each of the 100 independent runs, a maximum number of 2,70,000 LGA operations were generated on a single population of 150 individuals. The operator weights for crossover, mutation and elitism were maintained as default parameters (0.80, 0.02, and 1, respectively). The resulting 100 docked conformations were analyzed for binding energy, intermolecular energy and internal energy using Autodock wizard. The **5/6/7**-DNA complexes with highest binding affinity and lowest binding energy were selected and subjected for analysis of hydrogen bonding, hydrophobic and hydrophilic interactions. Chimera software was used to generate pictorial presentation of selected docked conformations.[35]

3. Results and discussion

3.1. Chemistry

Substituted benzimidazoles were synthesized earlier by us using silica supported periodic acid (H_5IO_6-SiO_2) as catalyst.[36] Herein, we synthesized 2-anthryl benzimidazoles (**5-7)** in good yields by coupling of 1,2-phenylenediamine with 9-anthraldehyde using similar methodology (Scheme 1). In order to increase the binding points in molecules, the synthesis of **6** and **7** was

accomplished by oxidative coupling of 3,4-diamino benzophenone and 3,4-diamino benzoic acid with 9-anthraldehyde in good yields. The obtained derivatives were characterized by IR, NMR and HRMS data.

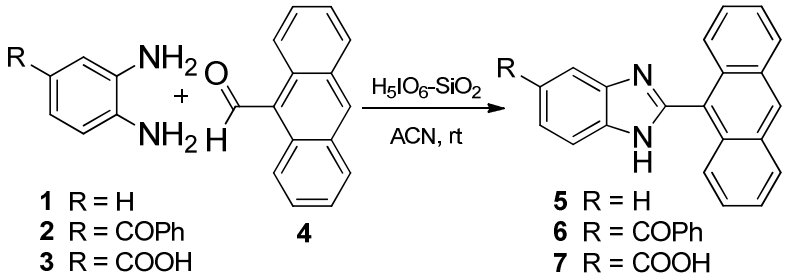

Scheme 1 Synthesis of benzimidazoles.

The ORTEP (Oak Ridge Thermal Ellipsoid Plot) of **5** obtained by single crystal X-ray structure is shown in Fig. 2 and the detailed parameters are given in Table 1S Supporting Information. The organization of the molecules in the crystal structure is completely dominated by the strong and classical N-H···N hydrogen bonding interaction. The *c*-glide related molecules generate helical chain structure through N2-H2N ···N1 interaction (H2N…N1 = 2.18 Å, N2…N1 = 2.998(8) Å and ∠ N2-H2N ···N1 = 158°) involving imidazole group.

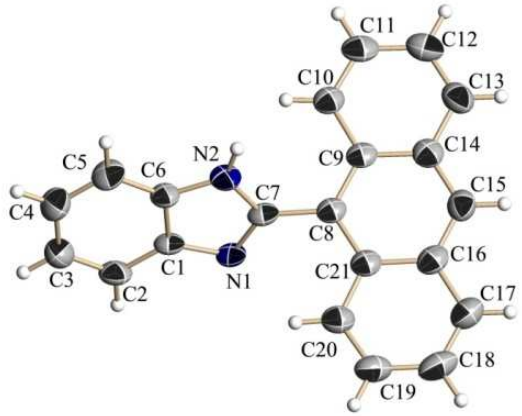

Fig. 2 ORTEP of compound **5**.

The neighboring chains along the crystallographic 2_1-screw axis are connected *via* off centered centrosymmetric C-H···π interactions, thus generating close packing of molecules (Fig. 3). Surprisingly, molecule being more hydrophobic comprising 4-phenyl rings does not associate through π···π interactions in its crystal structure. The C-H···π interactions which connect neighboring N-H···N linked chains across the inversion center are very off-centered and deviate from linearity (C2-H2···π(C9-C14); H2···Cg = 2.99 Å, C2···Cg = 3.742(10) Å, ∠ C2-H2···π (Cg) = 139°).

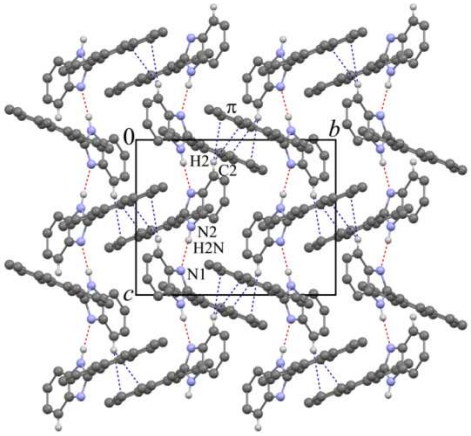

Fig. 3 Molecular packing viewed down *a*-axis showing association of helical chain via C-H···π interactions.

Molecular packing viewed down the *b*-axis revealed the generation of hydrophilic layer along the *c*-axis created by the alignment of benzimidazole moiety in layered fashion. Such adjacent hydrophilic layers were separated by the hydrophobic layer formed by the anthracene group moieties as seen in Fig. 4.

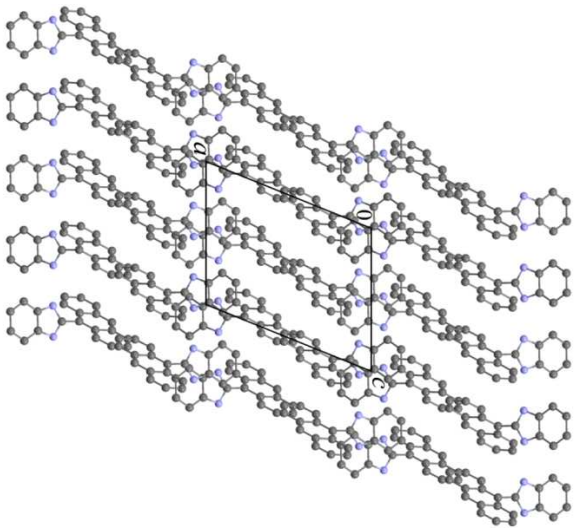

Fig. 4 Molecular packing viewed down b-axis showing formation of hydrophilic and hydrophobic layers.

3.2. DNA binding studies using ethidium bromide displacement assay

Ethidium bromide (EtBr) is a known DNA intercalator. Free EtBr exhibits low emission intensity in aqueous buffer solutions due to quenching by solvent molecules which is enhanced by stacking between DNA base pairs.[37] Therefore, if the compound binds to DNA more strongly than EtBr, then DNA-bound EtBr would get displaced leading to decrease in emission intensity.[38] In competitive EtBr binding studies (Fig.11S in Supporting Information), **5**-**7** was added to DNA pre-treated with EtBr ([CT-DNA]/[EtBr] = 15) and changes in emission intensity of EtBr-bound DNA as a function of added compound concentration were monitored. Compounds **5** and **6** exhibited least DNA binding affinity whereas **7** showed negligible reduction in emission of EtBr-bound DNA. This shows that **5**-**7** are interacting with DNA more through surface binding, and weakly through intercalative binding mode. The reason behind the low binding affinities of **5**-**7** can be rationalized with the help of single crystal x-ray structure of **5**

which shows rotation of anthracene ring through 60° along C(7)-C(8) bond. Due to disturbance in molecule planarity (shown in Fig. 5), there could be the hindrance in intercalation of anthracene ring into the DNA base pairs.

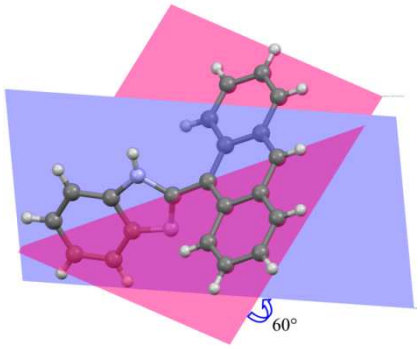

Fig. 5 ORTEP diagram of **5** displaying torsional difference between the two groups at the junction.

3.3. DNA photocleavage by compounds 5-7

The cleavage of plasmid DNA was monitored by agarose gel electrophoresis. When **5**-**7** were incubated with plasmid pBR322 DNA in dark, DNA cleavage was not observed. To optimize the UV irradiation time, the compounds were incubated at 37°C for 20 min before irradiation at 10, 20 and 30 min in the concentration range of 5 to 250 μM. At 250 μM and with 30 min irradiation, about 20% conversion of sc (supercoiled form I) into nc (nicked circular, form II) was observed (Fig. 10S in Supporting Information). Therefore, we increased the irradiation time up to 60 min and minimized the concentration to 50 μM. Irradiation of **5**-**7** at 364 nm for 1h under aerobic conditions resulted in the cleavage of sc form I of the plasmid pBR322 DNA to the nc form II (Fig. 6). Gradual increase in the amount of form II was observed with increased concentration of the molecules. However, the compounds exhibited different cleavage efficiency for the plasmid DNA. The compound **5** did not show any DNA cleavage

activity even at 100 μM, while **6** showed moderate activity, whereas **7** displayed maximum cleavage efficiency. This could be explained on the basis of stabilization of **7** on DNA helix through hydrogen bonding via COOH group thereby enhancing interaction.

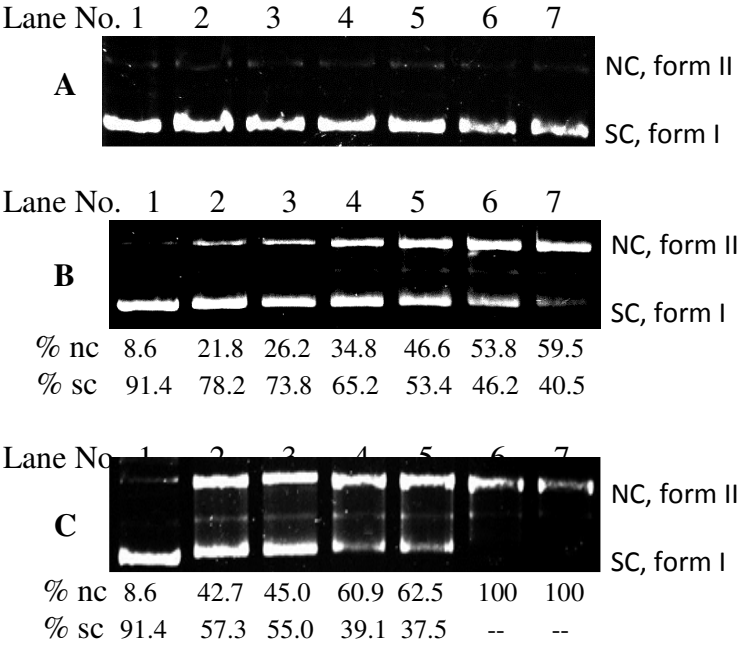

Fig. 6 Photocleavage of plasmid pBR322 DNA by (**A**) **5**, (**B**) **6** and (**C**) **7** on 20 min incubation at 37°C followed by 60 min irradiation (365 nm). [DNA] = 200 ng, Lane 1 = DNA Control, Lane 2-7= DNA+ **5**-**7** at 5, 10, 20, 30, 40 and 50 μM.

In order to understand the mechanistic aspect of the photo-induced DNA cleavage, **6** and **7** were studied in presence of different ROS (Reactive Oxygen Species) scavengers. It is known that type II DNA photocleavage reactions under aerobic conditions can proceed either through formation of singlet oxygen or through formation of hydroxyl or superoxide radicals. To ascertain the species involved in the DNA cleavage, **6** and **7** were incubated with DMSO (dimethyl sulphoxide), mannitol ($^{\cdot}$OH radical scavengers); DABCO (1,4-diazabicyclo[2.2.2]octane), NaN_3 (sodium azide), L-histidine ($^1O_2$ scavengers) and superoxide

dismutase (SOD, O_2^- scavenger). It was observed that cleavage of plasmid pBR322 DNA by **6** and 7 was inhibited by DABCO, NaN_3, L-histidine (Fig. 7, Lanes 5-7) indicating involvement of singlet oxygen in photocleavage of plasmid DNA. The results revealed that **7** possesses better DNA cleaving ability than **6** which can be attributed to additional hydrogen bonding interactions of **7** through carboxylate group with DNA backbone leading to increased localized concentration of ROS on photoirradiation.

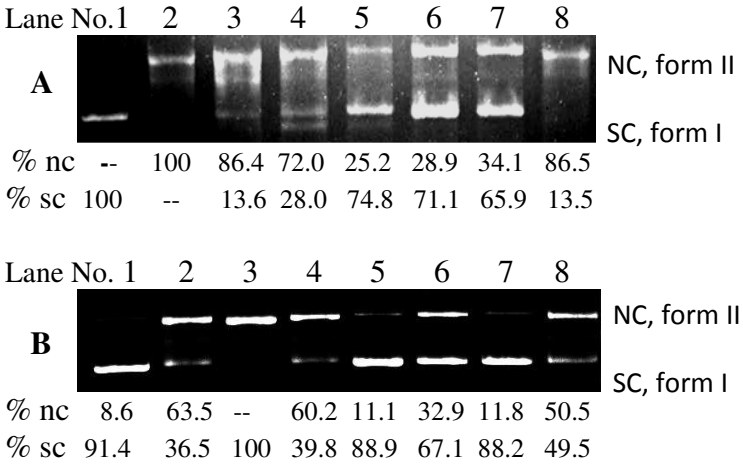

Fig. 7 Photograph of (1%) agarose gel showing the effect of inhibitors on cleavage of pBR322 plasmid DNA by **6** and **7** in TBE buffer (pH 8.2). (**A**) [**6**] = 40 μM, Lane 1, DNA control; lane 2, DNA+ **6**; lane 3, DNA+ **6** + DMSO; lane 4, DNA+ **6** + mannitol (50 mM); lane 5, DNA + **6** + DABCO (10 mM); lane 6, DNA+ **6** + L-histidine (20 mM); lane 7, DNA + **6** + NaN_3; lane 8, DNA+ **6** +SOD (15 units) and (**B**) [**7**] = 40 μM, Lane 1, DNA control; lane 2, DNA+ **7**, lane 3 DNA+ **7** + DMSO; lane 4, DNA+ **7** + mannitol (50 mM); lane 5, DNA + **7** + DABCO (10 mM); lane 6, DNA+ **7** + L-histidine (20 mM); lane 7, DNA + **7** + NaN_3; lane8, DNA+ **7** +SOD (15 units); [DNA]=200 ng.

3.4. Molecular Modeling

In-silico work has been performed in order to predict the conformational preferences of 2-anthryl substituted benzimidazole derivatives and to explore the mechanism of DNA cleavage by them.

3.4.1. Conformational preferences and molecular electrostatic potentials (MEPs)

To elucidate the conformational preferences and analysis of crystallographic features, automated complete geometry optimizations were carried out for **5**-**7** by semi-empirical, HF and DFT methods. In all optimization result, DFT method yields least energy stable conformation by preserving overall geometrical salient features from crystal structure of **5**. Therefore, we compared DFT optimized geometry for **5-7**. The calculation revealed that **6** is slightly fluctuated and energetically stable than **5** and **7,** whereas **7** is geometrically stable than **5** and **6**, as evidenced by torsion angles and intramolecular hydrogen bonding interactions (Figs. 13S, 14S in Supporting Information).

Molecular electrostatic potentials (MEPs) of **5**-**7** have been calculated using DFT method (Fig. 15S in Supporting Information). MEP maps show negative potential (red color) for O(1), O(2) and N(1) which might indicate that it serve as hydrogen bond acceptor, while the positive potential (blue color) associated with the hydrogen attached to N(2) and O(2) suggested its role in hydrogen bond donor. MEP results demonstrated that O(1), O(2), N(1) and N(2) are involved in interactions with DNA molecule as hydrogen bond acceptor/donor groups, whereas **6** with benzoyl substituent shows surface binding to DNA. It also suggests that **7** with carboxyl substituent is more interactive with DNA molecule than **5** and **6** (Table 2S in Supporting Information), thereby strongly involved in cleavage of DNA molecule, which is in line with our experimental observations.

3.4.2. Molecular docking with DNA

Molecular docking studies were carried out to explore binding of **5**-**7** with DNA. Complexes showing lowest energy were selected and subjected to geometrical parameter analysis such as hydrophobic; hydrogen bonding and van der Waals interactions (Table 3S in Supporting Information). Fig. 8 depicted docked complexes of **5**-**7** with DNA molecule. Crystal structure provides accurate structural and functional information of biomolecules and chemical compounds. The correct starting geometry is a success determine step in the computational studies. Determined 3D structure of benzimidazole plays significant role in exploring its structural consequences and conformational behavior during interaction with DNA molecule. Predicted hydrogen bonding and other non-covalent interactions between benzimidazole derivatives and DNA molecule may pave the way to elucidate structural features of benzimidazole. Therefore, known crystal structure is important factor in emphasize the inhibition mechanism of DNA by benzimidazole derivatives. The resulting least binding energies for **5**-**7** were found to be -9.12 kcal/mol, -11.64 kcal/mol and -9.24 kcal/mol respectively. All compounds were stacked with A-T rich region of DNA minor groove by surface binding interactions. In these docked complexes, intra and inter molecular H-bond interactions significantly participated in maintaining stacked position of compounds with DNA minor groove. Hydrophobic nature of benzoyl group in **6** may be involved in stacking interactions with DNA as shown in Fig. 8B. In docked complex of **7** (Fig. 8C), the geometry was completely flipped by 180° within DNA minor groove as compared to **5/6**-DNA complexes. This might be due to presence of strong interactions of carboxylic oxygen with G_{16}, A_{17} and A_{18} bases. Extra hydrogen bonding interactions were observed in case of **7**- DNA complex than **5/6**-DNA

complexes. Hydrogen bonding interactions for **5**-**7** with DNA was shown in Fig. 12S in Supporting Information.

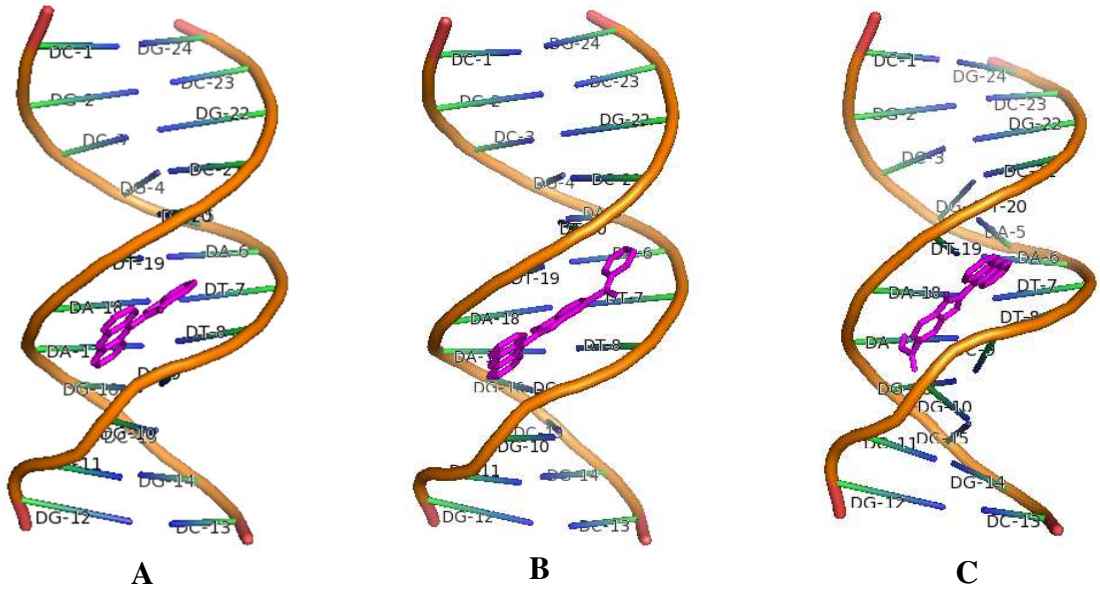

Fig. 8 Surface binding interactions of **5**-**7** with DNA molecule (1BNA) docked complexs.

3.5. Anticancer activity

The synthesized benzimidazoles **5**-**7** were tested for their anticancer activity against two cell lines MCF-7 and HL-60 by MTT colorimetric assay. The cells were treated with **5**-**7** for 48 h and the results are expressed as IC_{50} in µM considering viability of untreated cells to be 100% as summarized in Fig. 9. All the tested derivatives exhibited potent activity against MCF-7 and HL60, which was found to vary according to the substitution at 5^{th}-position of benzimidazole ring. The benzoyl substituted benzimidazole **6** showed highest potency (IC_{50}:16.18±0.07 µM for MCF-7 and 15.15±0.05 µM for HL-60), the carboxyl substituted benzimidazole **7** which was moderately potent (IC_{50}:19.21±0.08 µM for MCF-7 and 18.29±0.06 µM for HL-60),whereas **5** exhibited reduced activity (IC_{50}:20.48±0.08 µM for MCF-7 and 23.23±0.09 µM for HL-60)

Comparison of these values with that of cisplatin (IC_{50}:40.45±0.29 μM for MCF-7 and 41.08±0.32 μM for HL-60) indicated that all these compounds (**5-7**) are more potent than cisplatin under the present experimental condition.

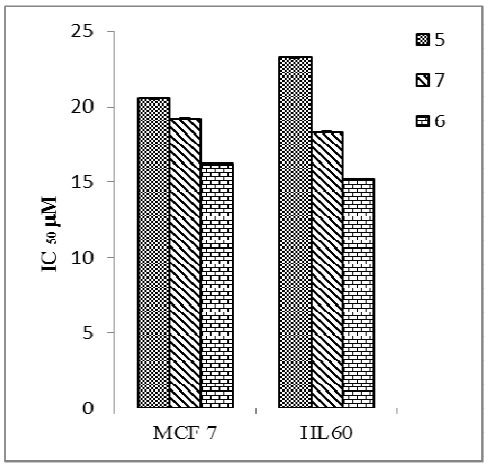

Fig. 9 IC_{50} in μM for **5-7** with MCF7 and HL60 cell line.

Cellular morphology after treatment with **6** and **7** was observed using fluorescence and confocal microscopy. As can be seen from Fig. 10, the total fluorescence intensity throughout the cell is quite high. After 48 h, fluorescence was found in the cytosol, mostly concentrated in the area close to the nucleus. No fluorescence was detected in the nucleus indicating that only a fraction of the compound binds with nuclear DNA which was supported by DNA binding studies using ethidium bromide displacement assay. The cells treated with **5** seem to be healthy with more localized fluorescence whereas **7** gives diffused fluorescence. Further, cells treated with **6** seem to form uniform granule like structures evenly distributed throughout cytoplasm with distinct morphological changes indicative of cell death, demonstrating the better potency by **6.**

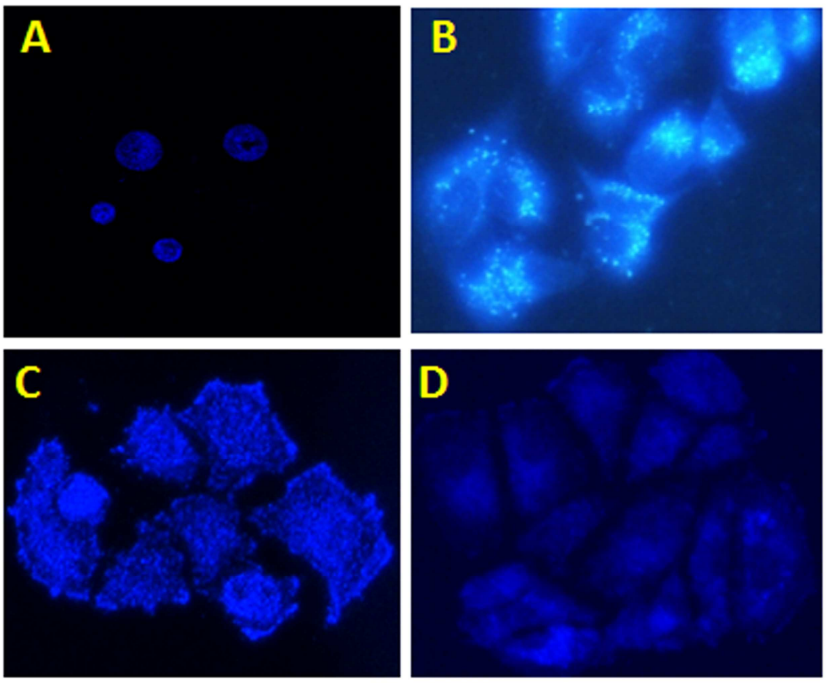

Fig. 10 Fluorescence microscopic images of MCF-7 cells showing cellular uptake after 24h incubation. A) Untreated control; B) treatment with 5; C) treatment with 6 and D) treatment with 7.

Intracellular fluorescence images are captured by confocal microscopy as shown in Fig.11. Panel a (1-3) shows bright field images of MCF7 cells: untreated control and treated with **6** and **7** respectively. In panel b (1-3), the nucleus is stained with DAPI. Cells in panel c (1-3) are stained with propidium iodide (PI) and panel d (1-3) shows the merged images and gives clear picture for MCF-7 cell line. Fluorescent and confocal images indicate the loss of membrane integrity of cells treated with **6.** However, membrane blebbing with simultaneous nuclear condensation and loss of distinct morphological features in the nuclear region in cells treated with **7** suggest cell death.

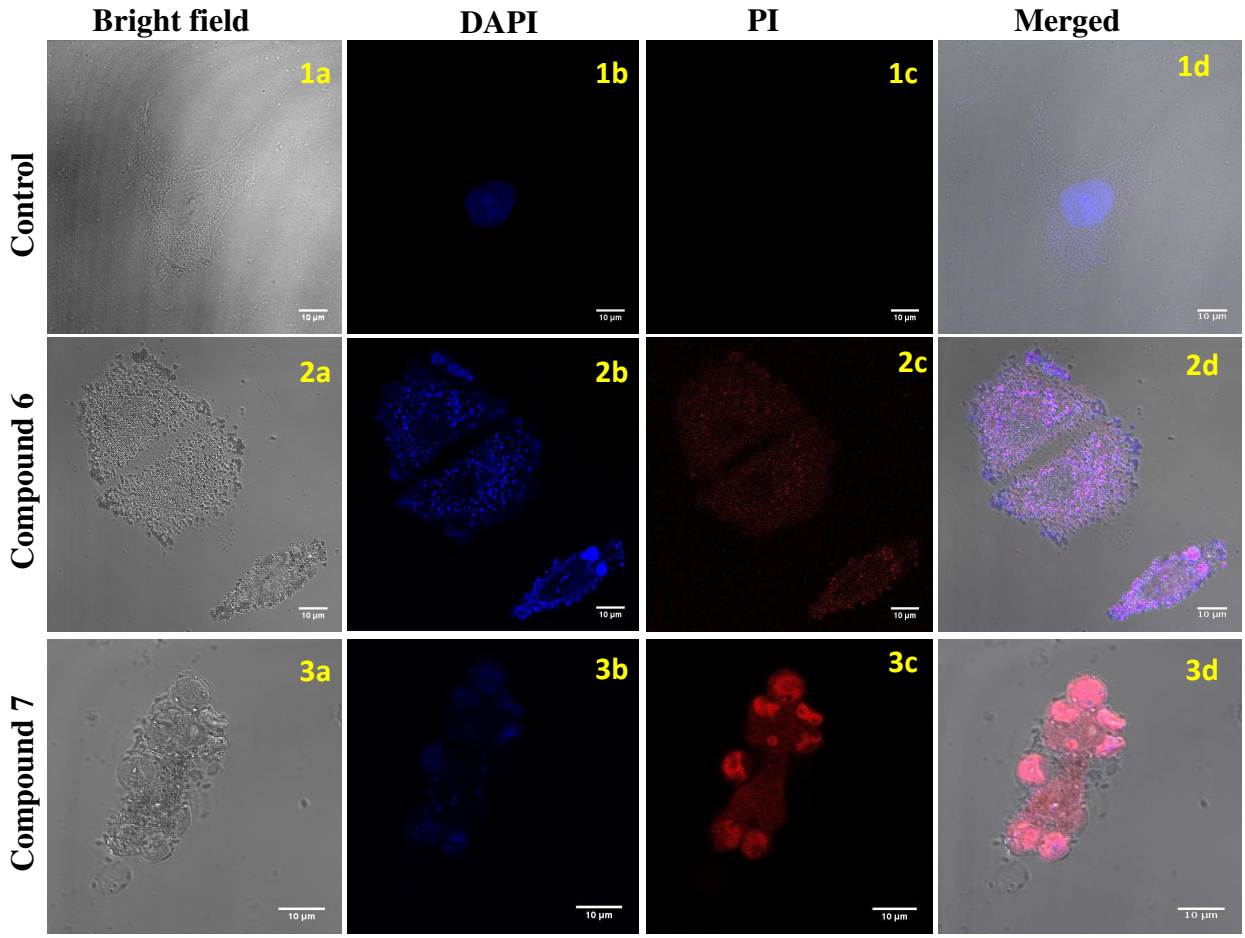

Fig. 11 Representative confocal micrographs of MCF7 cells (1a-d) untreated control bright field images; (2a-d) treated with **6**; (3a-d) treated with **7**.

Superior anticancer activity was shown by **6** when compared with **5** and **7**. This can be attributed to formation of energetically stable complex with DNA as well as better cellular permeability over other analogs. On the other hand, stabilization of **7** on DNA through H-bonding interaction as predicted in molecular docking studies, may have contributed to its slightly more photoinduced DNA cleavage activity.

4. Conclusions

2-Anthryl benzimidazole derivatives were synthesized in good yield. DNA cleavage activity was found to vary with substitution pattern. The carboxyl substituted derivative **7** showed greater DNA cleavages than **6**, while **5** did not show any DNA cleavage. The cleavage of pBR322 plasmid DNA by **6** and **7** was due to singlet oxygen species. DNA binding studies using ethidium bromide assay shows that **5**-**7** interact with DNA more through surface binding than intercalative binding mode due to non-planarity in the molecules. All benzimidazole derivatives (**5**-**7**) exhibited potent anticancer activity as compared to cisplatin against MCF7 and HL60 cell lines. The presence of benzoyl substitution at 5^{th}-position **6** was found to be more active as compared to the carboxyl substituted **7**, which is more active than **5**. Molecular docking study also suggests that **6** forms lowest energy (-11.64kcal/mol) stable complex with DNA. Theoretical study was found to be in line with experimental data. Cellular death by penetration of the test compounds vary with the substitution on the benzimidazoles, that was confirmed by confocal and fluorescence microscopy. Present synthesis, anticancer activity, DNA interaction and docking study may help for the development of more potent compounds in future.

Acknowledgements

VSS and VAS are thankful to Department of Science and Technology (DST), New Delhi for the financial support and Senior Research Fellowship (SR/S1/OC-89/2009) respectively. ANK acknowledges financial support from D. B. Limaye Trust. S. Ghosh thanks Council of Scientific and Industrial Research (CSIR) for Senior Research Fellowship.

Electronic Supplementary Information

Copies of ^{1}H and ^{13}C NMR spectrums of compound **5-7**. High concentration irradiation image of compound 5 and ethidium bromide displacement graph. Figures of H-bonding interactions of 5-7 with DNA, conventional numbering, automated complete geometry optimizations and molecular electrostatic potential. Tables for crystal structure data of 5, geometrical parameters and intra molecular H-bondings. Crystallographic data (cif) of compound **5** was given. Supplementary data related to this article can be found online at

References

1 (a) Y. Bansal, O. Silakari, *Bioorg. Med. Chem*., 2012, **20***,* 6208-6236. (b) R. P. Anthony, V. D. Rodrigo, S. K. Louis, C. D. John, B. T. Leroy, *J. Med.Chem*.,1998, **41,**1252-1262.

2 J. Chen, Z. Wang, C. M. Li, Y. P. Lu, K. Vaddady, B. Meibohm, J. T. Dalton, D. D. Miller, W. Li, *J. Med. Chem*., 2010, **53**, 7414-7427.

3 (*a*) L.Yun-Fei, W. Gui-Feng, H. Pei-Lan, H. Wei-Gang, Z. Feng-Hua, G. He-Yong, W. Tang, Y. Luo, F. Chun-Lan, S. Li-Ping, R. Yu-Dan, W. Lu, Z. Jian-Ping, *J. Med. Chem*., 2006, **49**, 4790-4794. (*b*) H. Banie, A. Sinha, R. J. Thomas, J. C. Sircar, M. L. Richards, *J. Med. Chem*., 2007, **50**, 5984-5993.

4 D. Sharma, B. Narasimhan, P. Kumar, A. Jalbout, *Eur. J. Med. Chem*., 2009, **44**, 1119-1127.

5 H. Goker, C. Kus¸ D. W. Boykin, S. Yildizc, N. Altanlar, *Bioorg.Med. Chem*., 2002, **10**, 2589-2596.

6 (*a*) E. Schneider, Y. H. Hsiang, L. F. Liu, *Adv. Pharmacol.*, 1990, **21**, 149-183. (*b*) A. Y. Chen, L. F. Liu, *Ann. Rev. Pharmacol. Toxicol.*, 1994, **34**, 191-218.

7 (*a*) T. A. Beerman, M. M. McHugh, R. Sigmund, J. W. Lown, K. E. Rao, Y. Bathini, *Biochem. Biophys. Acta.*, 1992, **1131,** 53-61. (*b*) A. Chen, C. Yu, B. Gatto, L. F. Liu, *Proceedings of the National Academy of Science U.S.A.*,1993, **90**, 8131-8135.

8 Q. Sun, B. Gatto, C. Yu, A. Liu, L. F. Liu, E. J. LaVoie, *Bioorg. Med. Chem.Lett*., 1994, **4**, 2871-2876.

9 J. S. Kim, B. Gatto, C. Yu, A. Liu, L. F. Liu, LaVoie, E. J. *J. Med. Chem*., 1996, **39**, 992-998.

10 Z. G. Li, Q.Yang, X. H. Qian, *Tetrahedron,* 2005, **61**, 8711-8717.

11 K. Szacilowski, W. Macyk, A. Drzewiecka-Matuszek, M. Brindell, G. Stochel, *Chem.Rev.,* 2005, **105**, 2647-2694.

12 M. R. Duff, W. B. Tan, A. Bhambhani, B. S. Perrin, J. Thota, A. Rodger, C. V. Kumar, *J. Phy. Chem*., B 2006, **110**, 20693-20701.

13 G. Malojcic, I. Piantanida, M. Marinic, M. Zinic, M. Marjanovic, M. Kralj, K. Pavelic,H. Schneider, *Org. Biomol. Chem*., 2005, **3**, 4373-4381.

14 B. Wilson, M. J. Fernandez, A. Lorente, K. B. Grant, *Tetrahedron*, 2008, **64**, 3429-3436.

15 Y. Huang, Y. Zhang, J. Zhang, D. W, Zhang, Q. S. Lu, J. L. Liu, S. Y. Chen, H. H. Lin, X. Q. Yu, *Org. Biomol. Chem.*, 2009, **7**, 2278-2285.

16 R. F. Pittillo, C. Willey, *Appl. Microbiol.,* 1969, **18**, 519-521.

17 W. A. Remers, T. P. Wunz, R. T. Dorr, D. S. Alberts, C. L. Tunget, J. Einspahr, S. Milton, *J. Med. Chem*.,1987, **30**, 1313-1321.

18 C. C. Cheng, R. K. Y. Zee-Cheng, *Med. Chem.,* 1983, **20**, 83-89.

19 I. E. Smith, *Cancer Treat. Rev*., 1983, **10**, 103-115.

20 H. Y. Yap, B. S. Yap, G. R. Blumenschein, B. C. Barnes, F. C. Schell, G. P. Bodey, *Cancer Res*., 1983, **43**, 1402-1404.

21 D. Saha, A. Saha, B. C. Ranu, *Green Chem.,* 2009, **11**, 733-737.

22 Bruker (2006). APEX2, SAINT, and SADABS. Bruker AXS Inc., Madison, Wisconsin, USA.

23 G. M. Sheldrick, *Acta Crystallographica*, 2008, **A64**, 112-122.

24 G. B. Rocha, R. O. Reire, A. M. Simas, J. J. P. Stewart, *J. Comput. Chem.,* 2006**, 27**, 1101-1111.

25 J. J. P. Stewart, *J. Comput. Chem.,* 1991*,* **12**, 320-341.

26 M. J. S. Dewar, W. Thiel, *J. Am. Chem. Soc.,* 1977, **99**, 4899-4907.

27 M. J. S. Dewar, E. G. Zoebsch, E. F. Healy, J. J. P. Stewart, *J. Am. Chem. Soc.,* 1985, **107**, 3902-3909.

28 M. M. Francl, W. J. Pietro, W. J. Hehre, J. S. Binkley, M. S. Gordon, D. J. Defrees, J. A. Pople, *J. Chem. Phys.,* 1982, **77**, 3654-3665.

29 A. D. Becke, *J. Chem. Phys.,* 1993, **98**, 5648-5652.

30 Y. Shao, et al., *Phys. Chem. Chem. Phys.,* 2006**, 8,** 3172-3191.

31 G. M. Morris, R. Huey, W. Lindstrom, M. F. Sanner, R. K. Belew, D. S. Goodsell, A. J. Olson, *J. Comput. Chem.,* 2009, **16**, 2785-2791.

32 M. A. Rizvi, S. Guru, T. Naqvi, M. Kumar, N. Kumbhar, S. Akhoon, S. Banday, S. K. Singh, S. Bhushan, G. Mustafa Peerzada, B. A. Shah, *Bioorg. Med. Chem. Lett.,* 2014, **24**, 3440-3446.

33 P. R. Markad, D. P. Sonawane, S. Ghosh, B A. Chopade, N. Kumbhar, T. Louat, J. Herman, M. Waer, P. Herdewijn, D. D. Dhavale, *Bioorg. Med. Chem.,* 2014, **22**, 5776-5782.

34 S. Ghosh, P. More, A. Derle, A. B. Patil, P. Markad, A. Asok, N. Kumbhar, A. Jabgunde, M. Shaikh, B. Ramanamurthy, V. S. Shinde, K. R. Pardesi, D. D. Dhavale, B. A. Chopade, *PLoS One*., 2014, **9**, e106039.

35 E. F. Pettersen, T. D. Goddard, C. C. Huang, G. S. Couch, D. M. Greenblatt, E. C. Meng, T. E. Ferrin, *J. Comput. Chem.,* 2004, **25**, 1605-1612.

36 V. A. Sontakke, S. Ghosh, P. P. Lawande, B. A. Chopade, V. S. Shinde, *ISRN Org. Chem.,* 2013, Vol. 2013, Article ID 453682, 1-7.

37 S. Satyanarayana, J. C. Dabrowiak, J. B. Chaires, *Biochemistry*, 1993, **32**, 2573-2584.

38 M. J. Waring, *J. Mol. Biol.*, 1965, **13**, 269-282.